Eur. Phys. J. B (2017) 90: 163
DOI: 10.1140/epjb/e2017-70567-0

THE EUROPEAN PHYSICAL JOURNAL B

Regular Article

Large scale spatio-temporal behaviour in surface growth

Scaling and dynamics of slow height variations in generalized two-dimensional Kuramoto-Sivashinsky equations

Vaidas Jukneviˇcius[a], Julius Ruseckas, and Jogundas Armaitis

Institute of Theoretical Physics and Astronomy, Vilnius University, Sauletekio al. 3, 10222 Vilnius, Lithuania

Received 25 September 2016 / Received in final form 20 February 2017
Published online 4 September 2017 –

Abstract. This paper presents new findings concerning the dynamics of the slow height variations in surfaces produced by the two-dimensional isotropic Kuramoto-Sivashinsky equation with an additional nonlinear term. In addition to the disordered cellular patterns of specific size evident at small scales, slow height variations of scale-free character become increasingly evident when the system size is increased. This paper focuses on the parameter range in which the kinetic roughening with eventual saturation in surface roughness and coarseness is obtained, and the statistical and dynamical properties of surfaces in the long-time stationary regime are investigated. The resulting long-range scaling properties of the saturated surface roughness consistent with the power-law shape of the surface spectrum at small wave numbers are obtained in a wider parameter range than previously reported. The temporal properties of these long-range height variations are investigated by analysing the time series of surface roughness fluctuations. The resulting power-spectral densities can be expressed as a generalized Lorentzian whose cut-off frequency varies with system size. The dependence of this lower cut-off frequency on the smallest wave number connects spatial and temporal properties and gives new insight into the surface evolution on large scales.

1 Introduction

Detailed understanding of surface growth physics has fueled several advances in science and technology, including more accurate dating in archeology [1], better integrated circuit technology [2], as well as production of novel materials [3]. In many cases of scientific and technological interest, the evolution of growing surfaces can be described by so-called *continuum models* that consist of nonlinear partial differential equations and often display rich and interesting dynamics [4]. Even though not all of this dynamics is currently accessible experimentally, it still is worthwhile to investigate, especially in the view of rapid experimental [5] and theoretical [6] progress.

The object of this study is a continuum surface growth model described by the two-dimensional *generalized* Kuramoto-Sivashisky equation with a single independent parameter α,

$$\partial_t h = -\nabla^2 h - \nabla^4 h - \alpha \nabla^2 (\nabla h)^2 + (\nabla h)^2 \,, \qquad (1)$$

considered in [7], that produces chaotically evolving disordered spatial patterns. Equations of this type (with and without added noise) have been successfully used as models for amorphous solid surface growth [8–10] and nanoscale pattern formation induced by ion beam sputtering (IBS) [11–15].

[a] e-mail: vaidas.juknevicius@tfai.vu.lt

Equation (1) in two spatial dimensions describes the evolution of a $(2+1)$-dimensional interface, i.e., a surface whose height $h(\boldsymbol{r}, t)$ is defined as a function on a two-dimensional plane $\boldsymbol{r} \in \mathbb{R}^2$ that is growing in the direction h perpendicular to that plane as time t goes by.

Numerical studies of equation (1) in one dimension have also been performed by Muñoz-García et al. [16], and a good correspondence to the IBS experiments has been found [17].

Equation (1) has the celebrated Kuramoto-Sivashinsky (KS) equation [18–21] as its special case when parameter $\alpha = 0$:

$$\partial_t h = -\nabla^2 h - \nabla^4 h + (\nabla h)^2 \,. \qquad (2)$$

The latter equation stands as a paradigmatic model for chaotic spatially extended systems and has been used to study the connections between chaotic dynamics at small scales and apparent stochastic behaviour at large scales [22–24]. Various generalizations and modifications of the KS equation (2) with local and non-local damping terms, anisotropy, and noise have been used to study pattern formation due to ion-beam erosion [25–30]. Equation (2) itself in one- and two-dimensional cases has been a subject of active research for about three decades, and its scaling properties have even been an object of controversy.

It has been suggested by Yakhot [31] and subsequently confirmed and reiterated by different authors (see, e.g. [22,23,32]) that the large-scale behaviour of the

deterministic KS equation (2) in the one-dimensional case can be described by a stochastic equation

$$\partial_t h = \nabla^2 h + (\nabla h)^2 + \eta \tag{3}$$

where η represents random uncorrelated Gaussian noise.

Equation (3) has become known as the Kardar-Parisi-Zhang (KPZ) equation [33]. It was originally proposed as a continuum model for surface growth due to ballistic deposition [34], since it showed the same dynamic scaling behaviour [35]. However, the correspondence between KS and KPZ in two-dimensions has led to disagreements by the same authors [23,32,36,37], because of the lack of conclusive analytical results. More recent results [24,38] tend to support the conjecture that KPZ and KS equations belong to the same universality class, although the numerical results for the deterministic (noiseless) KS are not conclusive due to the extremely long transient effects. Recent numerical results for the two-dimensional KS [7] with much longer simulation times show the same scaling properties of the saturated surface roughness as obtained by Manneville and Chaté [39] where the Edwards-Wilkinson (EW) [40] type of behaviour is observed. The EW regime is the pre-asymptotic (in terms of system size) behaviour, and is expected to cross over to the KPZ scaling at much larger system sizes [41], thus, further supporting the argument that the two-dimensional KS and KPZ equations, in the large size limit, belong to the same universality class. However [7], has reported a finite-size scaling behaviour that is different from both the EW and the KPZ scaling in the less researched generalized KS case (1) with $\alpha > 0$.

The purpose of this paper is to demonstrate in a wider parameter range the validity of the scaling relations for the surface roughness reported in the previous work [7], and to investigate the dynamics of the scale-free low-wavenumber spatial variations that these relations imply.

The article is structured as follows. After commenting on numerical methods and parameters used in the investigation, Section 2 demonstrates the initial transient kinetics of the surface roughness and eventual cross-over to the saturation regime observed in the investigated parameter range. Section 3 presents morphologies of surfaces produced by the generalized KS equation (1) in the saturated regime and presents results on the finite-size scaling of the saturated surface roughness. The analysis of temporal behaviour of the surface roughness for the KS case is demonstrated in greater detail in Section 4, and the results of the same analysis for the generalized-KS case are then given in Section 5. We conclude with a summary of our findings and propose several directions for future work in Section 6.

2 Surface roughness: transient kinetics and saturation

In this investigation, the equation (1) is solved numerically for different values of α using the *finite difference* method with periodic boundary conditions, the time step $\Delta t = 0.005$, and spatial discretization step $\Delta x = 0.71086127010534$. Such a seemingly bizarre number for the discretization step Δx is actually a good approximation of the value that is needed in order for the system with periodic boundary conditions to be able to contain hexagonal patterns that appear in some other versions of the generalized KS equation (see for example [25,30]). The equation is solved for system sizes L ranging from about 36 to about 711 (i.e., on the $N \times N$ lattices with N from 50 to 1000, where $L = N\,\Delta x$). Different methods of numerical solution for (1) are presented and compared in [42].

In the KS case ($\alpha = 0$), the evolving surfaces reach the regime where the dynamics is chaotic, but statistically stationary. This type of behaviour also persists for $\alpha > 0$, at least up to $\alpha = 5$. However, for larger values of α, this stationary chaotic behaviour gives way to non-stationary effects that prevent the saturation in the surface evolution. Indeed, in the limiting case when $\alpha \to \infty$ in (1), by rescaling h, one arrives at the conserved Kuramoto-Sivashinsky equation [43],

$$\partial_t h = -\nabla^2 h - \nabla^4 h - \nabla^2 (\nabla h)^2 \,, \tag{4}$$

which produces a non-stationary regime with ever increasing surface roughness due to the uninterrupted coarsening of the surface patterns. Thus, by increasing α, there must be a route from the stationary chaotic evolution to non-stationary coarsening behaviour. The coarsening behaviour for relatively larger parameter values (up to $\alpha = 50$) has been investigated in a one-dimensional case and, to some extent, in the two dimensional case [44]. Nonetheless, the long-time behaviour at the intermediate α values seems to be quite complicated and has not been studied in detail so far.

Even though negative α values do not follow from surface growth or erosion models (see, e.g. [9,15]), it is desirable to understand the dynamics in that range for completeness.

However, the range of negative α values available for investigation is limited. In our numerical simulations with $\alpha < -0.14$, we find that large local gradients in the surface emerge and grow. They eventually exceed the numerical capacity of the simulation, thus making the required long-time calculations unstable. The reason for this most likely are the so-called *cancellation modes* (see, e.g. [15,45]). Indeed, when $\alpha < 0$, the contributions of the nonlinear terms in (1) cancel each other out for some mode, so that the dynamics of this mode is governed only by the linear part of (1). If, moreover, the wave number of this mode belongs to the linearly unstable band, then its amplitude blows up exponentially, thus, causing the simulation to break down.

Therefore, this work focuses on the evolution of surfaces produced by (1) in a moderate range, $-0.12 \leq \alpha \leq 5$, of parameter values where the long time behaviour is stationary.

One of the most important quantities characterizing a surface [46,47] is the surface *roughness* $w(t)$, also called the *surface width*:

$$w(t) := \sqrt{\left\langle \left(h(\boldsymbol{r},t) - \bar{h}(t)\right)^2 \right\rangle_{\boldsymbol{r}}} \,. \tag{5}$$

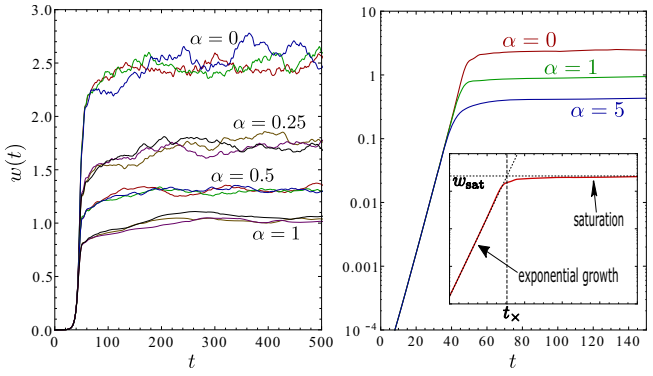

Fig. 1. Initial transient kinetics of the roughness $w(t)$, (5), of a surface evolving according to (1) with several values of parameter α. Each simulation starts from a random uncorrelated surface profile with initial roughness $w(0) = 10^{-4}$. The left panel shows $w(t)$ on linear scale for 3 realizations with each α. The right panel highlights the initial exponential increase of $w(t)$ by using a semi-logarithmic scale. The inset demonstrates the saturation roughness $w_{\rm sat}$ and the cross-over time $t_\times$.

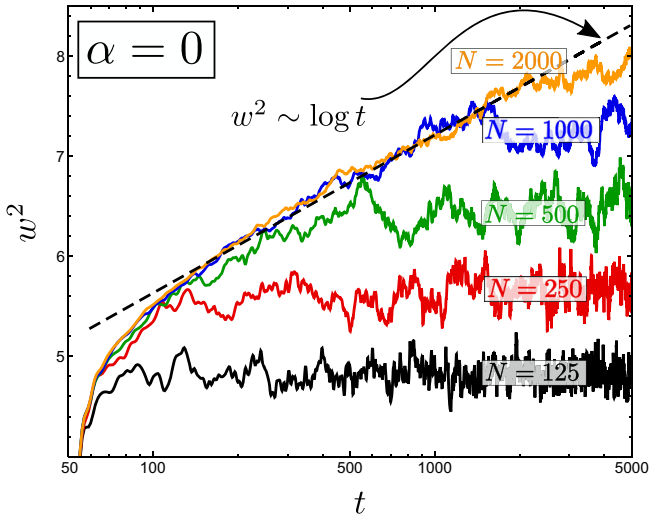

Fig. 2. Transient behavior of $w^2(t)$ (each curve is an ensemble average of 10 to 30 realizations) for $\alpha = 0$ and system sizes (in lattice units) $N = 125$ (black), $N = 250$ (red), $N = 500$ (green), $N = 1000$ (blue), $N = 2000$ (orange). Black dashed line corresponds to the logarithmic fit for the $N = 2000$ case. The corresponding system sizes L can be found from $L = N\Delta x$ where $\Delta x \approx 0.711$ is the spatial discretization step used in the simulations.

The scaling properties of this quantity are often used to characterize and classify various surface growth models into various universality classes [22,35,38,47]. The roughness of an evolving surface changes with time. In the range of parameter values considered here, the kinetics of $w(t)$ due to the surface evolution according to (1) seems to follow a distinct pattern (see, e.g. [7,9,10,43,48]): starting from a random surface with some small initial roughness $w(t = 0) \ll 1$, the roughness begins to grow at an exponential rate, but at some time $t_\times < 100$ this growth slows down significantly, and, eventually, crosses over to a stationary regime where it oscillates about some average (*saturation*) value $w_{\rm sat}$. This transient behaviour is shown in Figure 1 for several parameter values. For large enough systems another regime can be observed where $w(t)$ exhibits growth that is much slower than the initial exponential increase. For $\alpha = 0$ (KS case), this growth is approximately $w(t) \sim \sqrt{\log t}$, as shown in Figure 2 where the growth $w^2(t) \sim \log t$ appears as a straight line in the log-linear scale, which is consistent with pre-saturation behavior reported in [39]. The duration of this regime before finally reaching saturation increases with increasing system size which suggests that this growth is due to the development of large-scale height variations (see Sect. 3).

The value of saturated surface roughness can be defined as follows:

$$w_{\rm sat} = \lim_{T\to\infty} \left\langle w(t) \right\rangle_{t\in[t_0,\, t_0+T)} . \qquad (6)$$

Here $t_0 \gg t_\times$ is a time at which all initial transient effects have decayed and are virtually undetectable, i.e., the time at which the stationary regime has been reached. In practice, the total observation time T has to be much larger than the typical time scale in the kinetics of $w(t)$. In the investigation presented here, the saturation values for surface roughness $w_{\rm sat}$ are calculated using $t_0 = 2 \times 10^4$ and $T = 8 \times 10^4$. Note that these times are significantly larger than those recently achieved by Muñoz-Garcia et al. in the numerical investigation of an equation equivalent to (1) in the one-dimensional case [16,17]. There, although the "interrupted coarsening" is observed, the saturated stationary regime appears not to have been fully reached.

The surface roughness $w(t)$ represents the integral effect of all modes contributing to the surface morphology. Therefore, in this work, the time series of chaotic fluctuations of $w(t)$ in the stationary regime are used to investigate the long-time dynamics of surfaces, in particular, the temporal behaviour of the large-scale height variations observed in reference [7].

3 Surface morphologies and the scaling of roughness

The surface profiles produced by (1) in the stationary regime have a disordered cellular structure [7,9] (cf. Figs. 3 and 4). Since (1) is isotropic, and, consequently, the resulting profiles have no distinct direction on the $\boldsymbol{r}$-plane, the surface morphologies are investigated by averaging the surface height autocorrelation function over all directions at a distance $r = |\boldsymbol{r}|$:

$$C(r) = \left\langle \left\langle (h(\boldsymbol{r'}) - \bar{h})\,(h(\boldsymbol{r'}+\boldsymbol{r}) - \bar{h}) \right\rangle_{\boldsymbol{r'}} \right\rangle_{r=|\boldsymbol{r}|} . \qquad (7)$$

Figure 3 shows the resulting surface patterns and the corresponding normalized height correlation functions $C(r)/w^2$ for relatively small systems (of size $N = 200$, in lattice units) for different parameter α values. The shape of the autocorrelation function at smaller distances gives an insight into the small-scale surface patterns. For example, in Figure 3, one can see how the cellular patterns

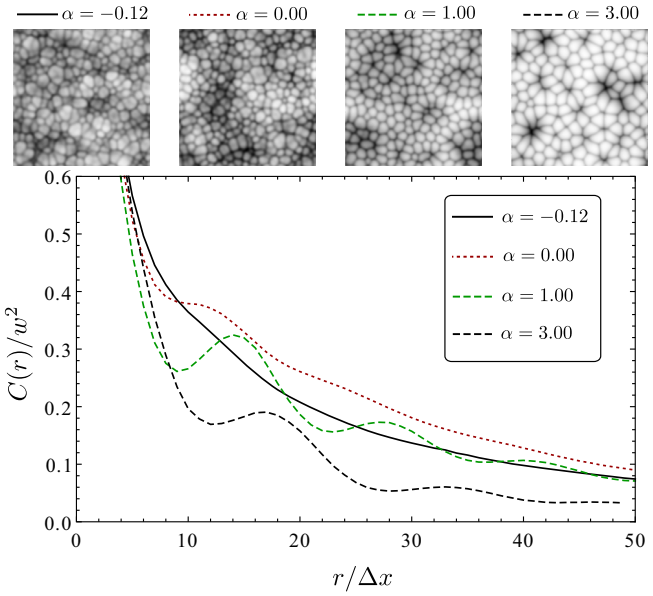

Fig. 3. Top panel: surfaces $h(\boldsymbol{r}, t)$ (values of the surface height h coded in gray-scale) evolving according to (1) at system size $N = 200$ ($L \approx 142$) with parameters $\alpha = -0.12, \ldots, 3$ at time $t = 10^5$ (in the stationary regime). Bottom panel: normalized autocorrelation functions $C(r)$ as defined in (7) of the surfaces that are shown in the top panel.

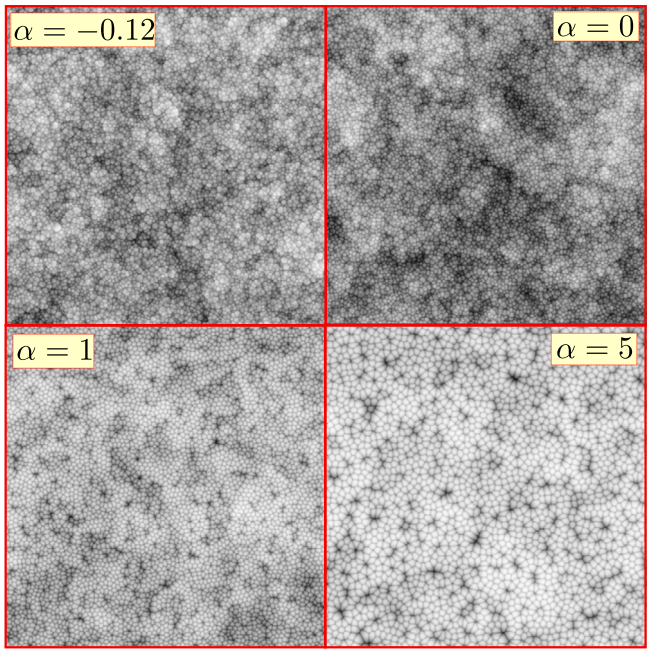

Fig. 4. Surfaces (values of the surface height h coded in gray-scale) for the system size $N = 1000$ ($L \approx 711$) evolving according to (1) with parameters $\alpha = -0.12, 0, 1, 5$ at time $t = 6 \times 10^4$.

change, by increasing α: the autocorrelation function (7) changes from monotonically decreasing at $\alpha = -0.12$ (corresponding to "flaky" surface profiles, with "flakes" of widely varying size) to having a short flat region at $\alpha = 0$ (corresponding to a profile with "cells" of similar size), and to a function with at least one distinct peak at $\alpha > 0$ whose distance increases with α (corresponding to the surface "cells" becoming almost round "humps" whose size increases with α).

Another thing that can be noticed in Figure 3 is that the normalized correlation function $C(r)/w^2$ decays slowly for $\alpha = 0$ and faster for increasing α. Also, perhaps surprisingly, the autocorrelation function for $\alpha < 0$ decays faster than for $\alpha = 0$. These are the first indications of the influence of parameter α on long-range height correlations.

Simulations show that the resulting saturated surface roughness (6) increases with the system size. This indicates that the surface profiles of larger systems contain additional spatial Fourier components of smaller wave number k, since the structure on smaller scales remains virtually unchanged [7].

Large-scale height variations in surfaces produced by (1) become more distinct as the system size is chosen to be many times larger than the typical cell size (see Fig. 4).

3.1 Scaling of roughness

The isotropic surface power-spectral density (PSD), $S(k)$, defined as the absolute square of the Fourier transform of the surface profile integrated over all directions of the wave vectors $\boldsymbol{k}$, can be obtained from the isotropic surface autocorrelation function $C(r)$ [7,49]:

$$S(k) = k\,2\pi \int dr\, r\, C(r)\, J_0(kr). \tag{8}$$

Here $J_0(kr)$ is the Bessel function of the first kind:

$$J_0(kr) = \frac{1}{2\pi} \int_0^{2\pi} d\phi\, e^{\mathrm{i}kr\cos\phi}. \tag{9}$$

Examples of numerically calculated surface PSD $S(k)$ using (7)–(9) for $\alpha = 0$ and $\alpha = 1$ can be found in [7]. There, one can see a distinct peak that corresponds to an average size of a hump-shaped cells in the surface pattern (see Figs. 3 and 4), and a power-law trend for small wave numbers.

The integral of the PSD $S(k)$ (8) over all wave numbers k equals the variance of the surface profile which is the square of surface roughness:

$$\frac{1}{2\pi} \int dk\, S(k) = w^2. \tag{10}$$

Since the surfaces in numerical simulations are represented on a discrete $(N \times N)$ lattice of finite size L with a discretization step Δx, wave numbers that can fit into the system are $k_n = n\Delta k$ with $n = 1, \ldots, N$ and $\Delta k = 2\pi/L$. For large enough systems with $N \gg 1$, according to (10), the square of the surface roughness can then be expressed as:

$$w^2 \approx \frac{1}{2\pi} \int_{k_{\min}}^{k_{\max}} dk\, S(k)\ , \tag{11}$$

where

$$k_{\min} \approx \frac{2\pi}{L} = \frac{2\pi}{N\Delta x}\,, \quad k_{\max} \approx \tfrac{2\pi}{\Delta x}\,.$$

If the discretization step Δx is kept constant (implying $k_{\max} = \text{const}$), and the surface patterns at different system sizes L (up to the smallest wave number $k_{\min} \propto L^{-1}$) remain statistically the same, then, by increasing the system size L, the calculated dependence $w^2(L)$ should yield, according to (12), the shape of the surface PSD $S(k)$ for small wave numbers $k \to 0$.

In [7], an assumption was made that the PSD $S(k)$ (8) of surfaces produced by (1) has a power-law shape for small wave numbers (below some value k_s):

$$S(k) = C\,k^{-\gamma} \;\text{ for }\; k < k_s\,. \tag{12}$$

By substituting (12) into (11), one gets three qualitatively distinct scaling behaviours $w^2(L)$ for $L > 2\pi\,k_s^{-1}$, depending on the value of spectral exponent γ in (12):

$$\begin{cases} w^2(L) = C_1 - C_2\,L^{-(1-\gamma)} & \text{for } \gamma < 1 \\ w^2(L) = C\ln L + B & \text{for } \gamma = 1 \\ w^2(L) = D_1 + D_2\,L^{\gamma-1} & \text{for } \gamma > 1. \end{cases} \tag{13}$$

For asymptotically large systems $L \to \infty$, (13) would become

$$\begin{cases} w^2(L) \sim \text{const} & \text{for } \gamma < 1 \\ w^2(L) \sim \ln L & \text{for } \gamma = 1 \\ w^2(L) \sim L^{\gamma-1} & \text{for } \gamma > 1\,, \end{cases} \tag{14}$$

corresponding to asymptotically constant roughness for $\gamma < 1$, logarithmically increasing square of the surface roughness for $\gamma = 1$, and power-law scaling for $\gamma > 1$.

It has been shown in [7] that the assumption (12) of a power-law surface PSD with $(0 < \gamma \leq 1)$ at small wave numbers is indeed valid for surfaces produced by (1) with parameter values $0 \leq \alpha \leq 1$, since the relations (13) fit the numerically calculated surface roughness exceptionally well.

Investigations of a broader parameter range, $-0.12 \leq \alpha \leq 5$, presented in this paper, show that the same assumption (12) also holds for other parameter values. Figure 5 shows the calculated square of the surface roughness w^2 dependence on the system size $L = N\Delta x$. In order to fit the results with different α values in the same plot, the numerical results and their fits for each α have been divided by the corresponding w^2 values at $N = 250$. At $\alpha = 0$ the resulting spectral exponent $\gamma = 1$ gives the logarithmic dependence $w^2(N)$ (see (13)) which is a straight line in the log-linear scale. This scaling is the same as found by Manneville and Chaté for the two-dimensional KS equation [39] and corresponds to the EW type of behaviour [40] which is the pre-asymptotic to the KPZ scaling [41].

As the parameter increases from $\alpha = 0$ to $\alpha = 5$, the γ values are found to decrease from $\gamma = 1$ to $\gamma \approx 0.55$ (see Fig. 5). This corresponds to slower-than-linear growth of w^2 with $\ln N$. Hence, for large systems w^2 approaches a finite value. Perhaps unexpectedly, for $\alpha < 0$, the exponent γ has also been observed to become smaller than 1.

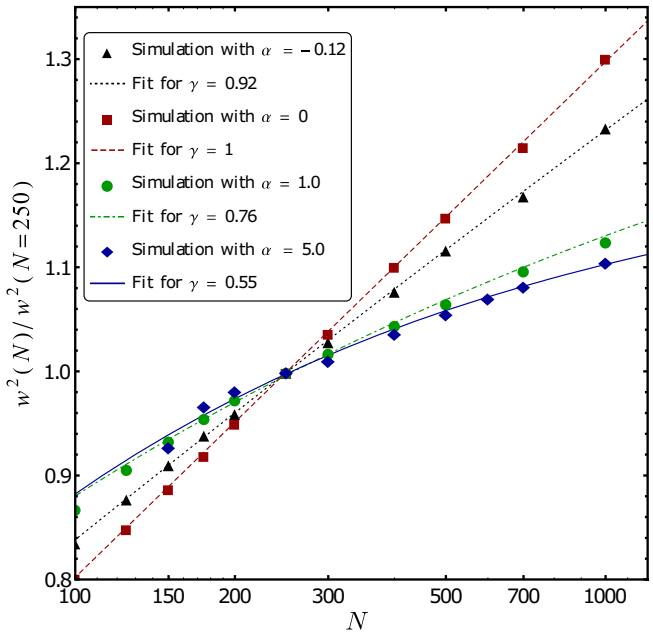

Fig. 5. (Log-linear scale) Time averaged square of the normalized surface roughness w^2 plotted as a function of the system size N (in lattice units). Symbols: numerical results for surfaces evolving according to (1) with different α values. Lines: fits of the numerical results by (13).

Therefore, we conclude that, in the range of system sizes considered, the scaling properties of the generalized KS equation (1) differs from those of the EW (and KPZ) equation. when $\alpha \neq 0$.

This seemingly different scaling for $\alpha \neq 0$ must be the effect of the finite system size L, since it can be shown using renormalization group (RG) arguments (see, e.g. [47]) that the influence of the nonlinear term $\nabla^2(\nabla h)^2$ has to become irrelevant at asymptotically large scales (when $k \to 0$), and the scaling for $L \to \infty$ has to be equivalent to the KS $\alpha = 0$ case. However, the present results suggest that this asymptotic regime is far from being reached for the systems in the range of sizes investigated here. The obvious influence of parameter α value on the scaling properties is most likely caused by the underlying change in the small-scale surface patterns (see Fig. 3) that interfere with the slow height variations of universal character. This would suggest that, in some practical cases, *different scaling properties* might be observed from those predicted by the RG arguments, even for relatively large systems.

4 Analysis of roughness dynamics in the Kuramoto-Sivashinsky case

Model equation (1) produces disordered spatial patterns that evolve in time. As shown in Section 3, with an increase of the system size L new long range height variations appear in the resulting surface profiles in addition to the small scale patterns. The apparent scale-free character of these slow height variations is very different from the

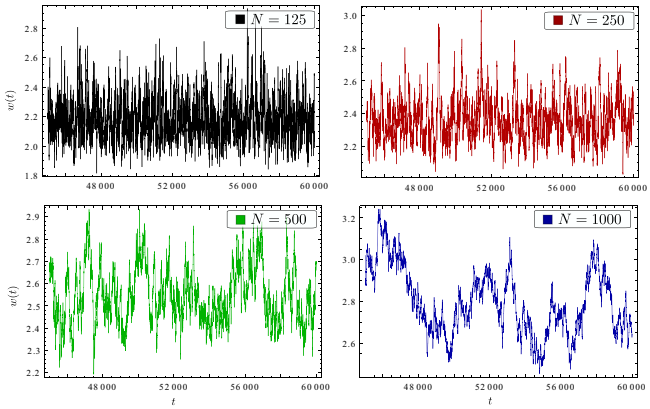

Fig. 6. Time series of the surface roughness $w(t)$, $t \in [4.5 \times 10^4, 6 \times 10^4)$ for $\alpha = 0$ and different system sizes N (in lattice units).

cellular patterns on small scales which have a characteristic length (the average size of a "cell" or "hump"). Also, the spatial properties of both, the small scale patterns and the large scale height variations, depend strongly on the value of parameter α in (1). This section investigates the corresponding dynamics of these surfaces.

In order to understand the complex spatio-temporal behaviour of (1), we investigate the dynamics of surfaces it produces by analysing the numerically obtained time series of the surface roughness $w(t)$ which contains the collective behaviour of all modes. The time series of $w(t)$ are investigated in the time interval $t \in [2 \times 10^4, 10^5)$ with sampling time $\tau_{\text{sample}} = 1$ (i.e., sampled every 200 time steps $\Delta t = 0.005$), that is, 8×10^4 values in total for every realization. The results are averaged over 5 to 10 realizations (differing in the initial surface profile) for every parameter α value. For the range of parameter values explored here, the surface evolution can be considered stationary and ergodic, since the statistical properties of $w(t)$ (average, standard deviation, skewness, autocorrelation function) seem to vary little from realization to realization. Moreover, their values calculated in large enough subintervals of the total time interval differ only slightly from each other.

In this section, the analysis of $w(t)$ is presented in more detail for parameter value $\alpha = 0$, that is, the Kuramoto-Sivashinsky case (2). The same analysis performed on other parameter values is discussed in Section 5.

4.1 Occurrence of slow modes

Figure 6 shows a representative sample of a surface roughness $w(t)$ time series for $\alpha = 0$ and system sizes varying from $N = 125$ to $N = 1000$. Even though the roughness dynamics is dominated by white noise for small systems ($N = 125$), additional slow modes appear as the system size is increased. For relatively large systems ($N = 1000$), the time series in question is similar to a signal produced by a random walk.

This transition can be visualized even more clearly by using the recurrence plot technique [50–53] (see Fig. 7).

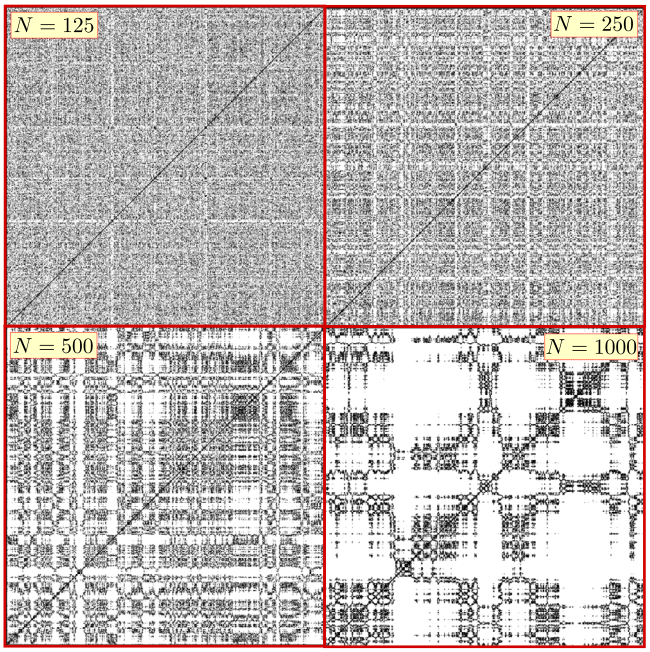

Fig. 7. Recurrence plots of the one-dimensional time series of the surface roughness $w(t)$ for $t \in [8 \times 10^4, 10^5)$, $\alpha = 0$, and different system sizes N (in lattice units). Here $\epsilon = 0.002\,\sigma$, where σ is the standard deviation from the average of the corresponding time series for each N.

There, a time series $s(t)$ is depicted by plotting a matrix $\boldsymbol{R}_{t_i,t_j}$. In the plot, the axes represent the discrete time t_i and t_j. A black dot ($\boldsymbol{R}_{t_i,t_j} = 1$) is put at a point (t_i, t_j) if the values of the time series $s(t)$ at these times coincide (recur) to a given accuracy ϵ. The pixel remains white otherwise (value $\boldsymbol{R}_{t_i,t_j} = 0$), that is:

$$\boldsymbol{R}_{t_i,t_j} = \Theta(\epsilon - |s(t_i) - s(t_j)|), \tag{15}$$

where $\Theta(x)$ is the Heaviside step function. Each of the recurrence plots in Figure 7 is made for a single realization of $w(t)$ in the time interval $t \in [8 \times 10^4, 10^5)$, i.e., one fourth of the total length of the time series is investigated.

The slow fluctuations of $w(t)$ that appear when the system size is increased can be attributed to the low wave number spatial modes that occur in larger systems. By investigating the scaling properties of these fluctuations, connections between spatial and temporal properties of the corresponding large scale height variations can be made.

4.2 Autocorrelation functions

The character of the slow fluctuations that appear in the time series (TS) of the surface roughness $w(t)$ resulting from (1) for large systems (see Figs. 6 and 7) is captured by their autocorrelation functions,

$$A(\tau) = \big\langle (w(t) - \bar{w})(w(t+\tau) - \bar{w}) \big\rangle_t, \tag{16}$$

where $\bar{w} = \langle w(t) \rangle_t$ is the average value of $w(t)$ in the stationary regime. Figure 8 shows the autocorrelation

functions obtained from TS of $w(t)$ with $\alpha = 0$ for four different system sizes increasing by the factor of 2: $N = 125, 250, 500, 1000$. In the top panel of Figure 8, the normalized (i.e., divided by the variance $\sigma_w^2 = \langle (w(t) - \bar{w})^2 \rangle_t \equiv A(0)$) autocorrelation functions are displayed in the log-linear scale. In this plot, one can immediately recognize the way in which the characteristic time scales in $w(t)$ grow with N. For instance, by defining some characteristic correlation time $\tau_{\rm corr}$ as, for example, the lag τ at which the autocorrelation function decays to the 10% (dashed horizontal line) of its initial value at $\tau = 0$, i.e.,

$$\tau_{\rm corr} = \min\{\tau > 0 \,|\, A(\tau)/\sigma_w^2 \leq 0.1\}, \tag{17}$$

one can see that it increases by about the same factor (corresponding to almost constant shifts along a logarithmic scale of τ axis) as the system size N increases by a factor of 2. This indicates that the characteristic time $\tau_{\rm corr}$ grows as a power law of N:

$$\tau_{\rm corr} \propto N^{\xi}. \tag{18}$$

Further insight into the dynamics can be gained by looking at the same autocorrelation functions in a semi-logarithmic plot, as displayed on the bottom panel of Figure 8. Plotted this way, the autocorrelation functions $A(\tau)$ appear almost as straight lines (with an additional kink at very small τ) indicating that the their shape should be approximately exponential:

$$A(\tau) \approx \sigma_w^2 \, e^{-\lambda|\tau|}. \tag{19}$$

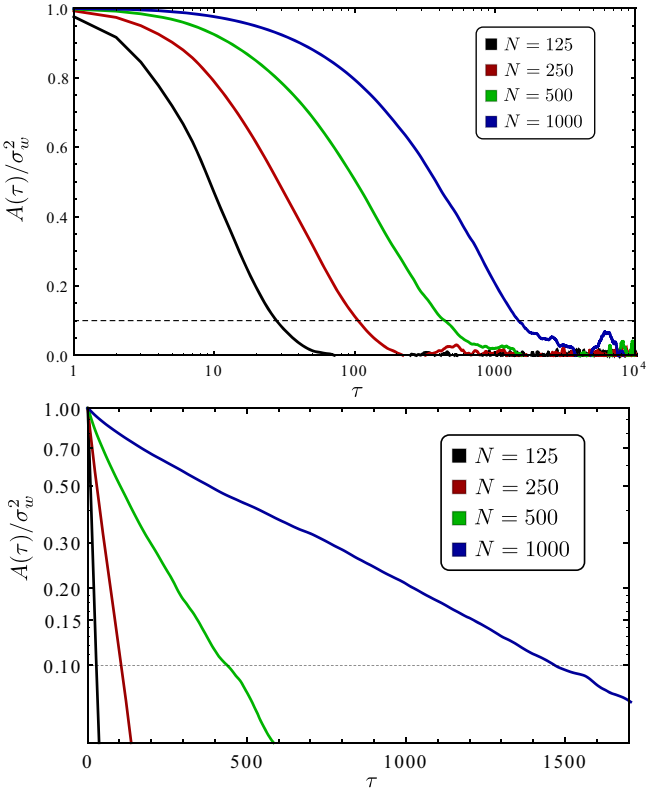

Fig. 8. Normalized autocorrelation functions $A(\tau)$ of the surface roughness $w(t)$, $t \in [2 \times 10^4, 10^5)$ for $\alpha = 0$ and different system sizes (in lattice units) N. Top panel: log-linear scale. Bottom panel: semi-logarithmic scale. Horizontal dashed and dotted lines in both panels represent the $A(\tau)/\sigma_w^2 = 0.1$.

4.3 Power spectra and characteristic frequencies

In order to obtain more quantitative results, it is essential to look at the shape of the corresponding power spectra of $w(t)$. As stated by the Wiener-Khinchin theorem [54], the power spectral density (PSD) $W(f)$ of a signal can be obtained by Fourier transforming its autocorrelation function (16):

$$W(f) = \int_{-\infty}^{\infty} d\tau \, A(\tau) \, e^{-i2\pi f \tau}. \tag{20}$$

By substituting the exponentially decaying autocorrelation function $A(\tau) \propto e^{-\lambda|\tau|}$ (as in (19)) into (20), the PSD $W(f)$ of a Lorentzian shape is obtained:

$$W(f) \propto \frac{f_0}{f_0^2 + f^2}, \tag{21}$$

where $f_0 = \lambda/2\pi$ is the characteristic frequency that signifies the cross-over between different behaviours of $W(f)$, namely:

$$W(f) \sim \begin{cases} \text{const} \ , & f \ll f_0, \\ f^{-2} \ , & f \gg f_0. \end{cases} \tag{22}$$

Thus, f_0 represents the lowest frequency (or the lowest decay rate $\lambda \propto f_0$) that affects the dynamics of $w(t)$. The above considerations suggest that f_0 must correspond to the lowest wave number, $k_{\rm min} \propto L^{-1}$, of a spatial mode occurring in the system of size L.

Plotted in semi-logarithmic scale (bottom panel of Fig. 8), the autocorrelation functions $A(\tau)$ appear as almost straight lines corresponding to the approximate exponential decay (19) whose PSD is a Lorentzian (21). Nevertheless, there are deviations from this trend at very short lag times τ. These deviations correspond to additional fluctuations with a very short correlation time – a *white noise* whose PSD is a constant. Therefore, the resulting PSD of $w(t)$ can be fitted by a Lorentzian plus a constant:

$$W_{\rm fit}(f) = \frac{A}{f_0^2 + f^2} + B \tag{23}$$

where A, B and f_0 are fit parameters.

The PSDs obtained from the autocorrelation functions of the surface roughness at $\alpha = 0$ for different system sizes $N = L/\Delta x$ are shown in the top panel of Figure 9 together with their fits by (23). A closer analysis shows that a function with a generalized Lorentzian plus a constant B,

$$W_{\rm fit}(f) = \frac{A}{(f_0^2 + f^2)^{\beta/2}} + B \, , \tag{24}$$

with $\beta = 1.8$ fits the calculated PSDs even better, see the bottom panel of Figure 9. Note that β is *not* the growth

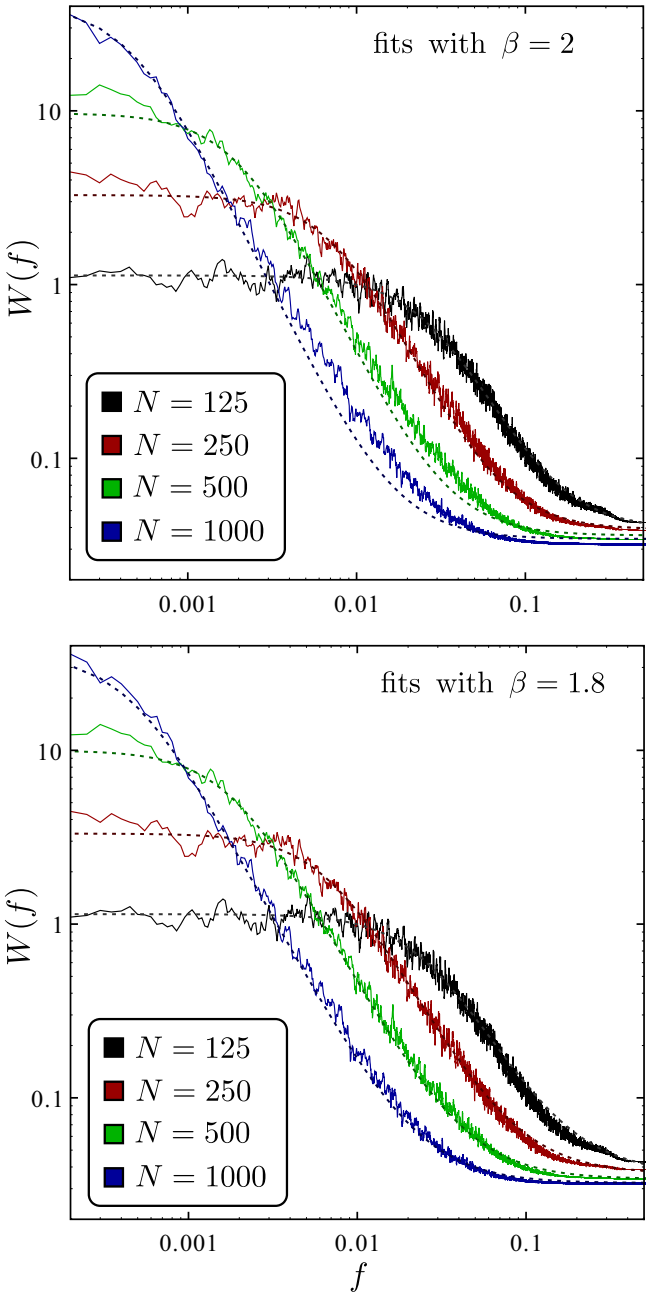

Fig. 9. The power spectral densities $W(f)$ of the surface roughness $w(t)$ for $t \in [2 \times 10^4, 10^5)$, $\alpha = 0$, and different system sizes N. Solid lines: calculation results of (20) with (16). Dotted lines: fits of the calculated results by (24) with $\beta = 2$ (top panel) and $\beta = 1.8$ (bottom panel).

critical exponent, as opposed to the usual kinetic roughening nomenclature [47].

The cross-over frequency f_0 obtained as a fit parameter represents the lowest frequency (corresponding to the longest time scale) in the kinetics of $w(t)$. In Figure 9, it is clearly visible that f_0 decreases as the system size N is increased. Since the lowest wave number $k_{\min}$ of the spatial modes occurring in the system is inversely proportional to the system size, $k_{\min} \propto N^{-1}$, the $f_0(N)$ dependence

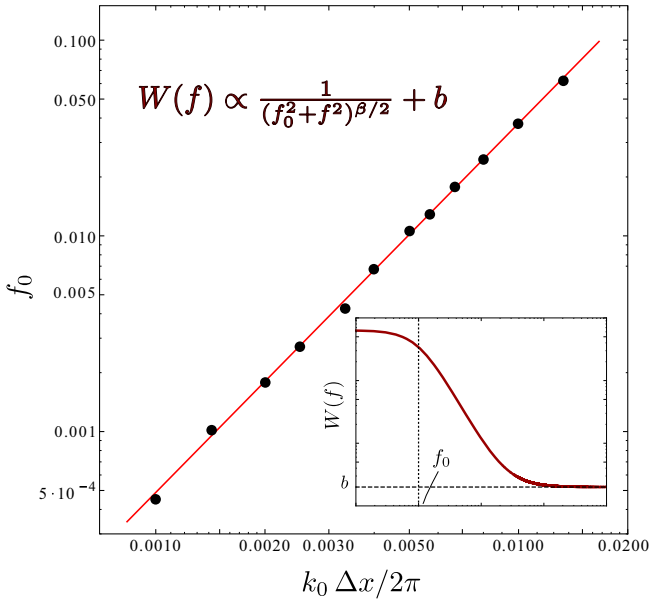

Fig. 10. (Log-log scale) Relation between the lowest frequency f_0 and the lowest wave number k_0 occurring in the system for $\alpha = 0$. The black filled circles are f_0 values obtained as fit parameters for numerical results by (24). The solid red line is the power-law fit $f_0 \propto k_0^{\xi}$ with $\xi \approx 1.89$. The inset on the bottom right shows f_0 for the PSD $W(f)$ defined by the expression shown on the top left.

connects the spatial and the temporal scales. Indeed, by defining the some critical wave number k_0 as

$$k_0 = \frac{2\pi}{L} \equiv \frac{2\pi}{\Delta x}\,\frac{1}{N} \propto k_{\min}, \tag{25}$$

one can obtain a dispersion relation $f_0(k_0)$ – a connection between the lowest wave number in the system and its corresponding frequency. The resulting f_0 dependence on $k_0 \Delta x/(2\pi) = N^{-1}$ for $\alpha = 0$ is shown in Figure 10 in the double-logarithmic scale. Plotted this way, the results appear to lie on a straight line, meaning that the relation is approximately a power-law $f_0 \propto k_0^{\xi}$ with the exponent $\xi \approx 1.89$, as the fit shows (cf. Fig. 10).

5 Dynamics of roughness for other parameter values

The fluctuations of $w(t)$ change character as parameter α is varied. This can already be seen from their time series (Fig. 11). This section presents some of the results on spatio-temporal properties of surfaces evolving according to (1) with parameter values $\alpha \neq 0$ in order to point out the similarities and differences from the $\alpha = 0$ case presented in Section 4.

5.1 Spatio-temporal properties

The same type of analysis, as presented in Section 4 for parameter $\alpha = 0$, has also been performed for other parameter values.

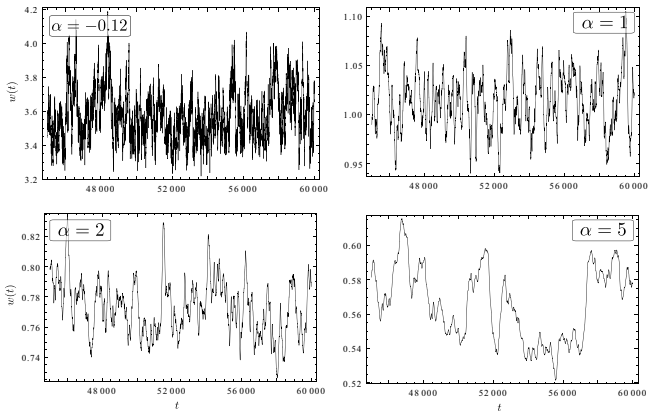

Fig. 11. Time series of the surface roughness $w(t)$ for $t \in [4.5 \times 10^4, 6 \times 10^4)$, system size $N = 500$ (in lattice units), and different values of parameter α.

As in the $\alpha = 0$ case, for $\alpha \neq 0$, the occurrence of slow modes can also be observed as the system size increases. However, since the character of low wave number spatial variations depends on α, as shown in Section 3, their temporal properties also differ.

The PSDs of $w(t)$ for $-0.12 \leq \alpha \leq 5$ can be fitted very well (see Fig. 15) by a generalized Lorentzian with an added constant (24) at different system sizes N (except for some cases discussed in the following subsection). The exponent β in the fit (24) increases monotonically from $\beta \approx 1.7$ for $\alpha = -0.12$ to $\beta \approx 3$ for $\alpha = 5$. From these fits at different system sizes N, the relations between the lowest frequencies f_0 in the dynamics and lowest wave numbers of spatial variations $k_0 \propto N^{-1}$ are obtained (Fig. 12), as is done in Section 4 for $\alpha = 0$.

Figure 12 reveals how the spatio-temporal behaviour of evolving surfaces depend on parameter α.

The relations $f_0(k_0)$ shown in Figure 12 indicate that for small k_0, the power-law behaviour $f_0 \sim k_0^{\xi}$ observed in Figure 10 for $\alpha = 0$, also persists for $\alpha \neq 0$ with exponent ξ decreasing with increasing α: from $\xi \approx 2.2$ for $\alpha = -0.12$ to $\xi \approx 0.9$ for $\alpha = 2$. This power-law trend can be attributed to the dynamics of scale-free height variations, and the change of the exponent ξ with α can most likely be related to the corresponding change of the surface scaling properties (Sect. 3).

However, for $\alpha \neq 0$, this power-law behaviour flattens out at larger values of k_0 corresponding to small scales. This cut-off of the power-law trend is most likely due to the coarser small-scale patterns produced by larger values of α (see Fig. 3) whose slower dynamics begins to overshadow, at smaller scales, the dynamics of scale-free height variations corresponding to the power-law trend.

For $\alpha = 5$ (not shown in Fig. 12), the possible power-law behaviour is more difficult to determine, since the curve $f_0(k_0)$ appears flat almost through the whole range of k_0, except for only two points with smallest k_0 – way less than enough to make conclusions.

One can interpret f_0 at some $k_0/2\pi = l_0^{-1}$ as the approximate rate of processes at the length scale l_0, or $n_0 \equiv l_0/\Delta x$ in lattice units. Then the results displayed

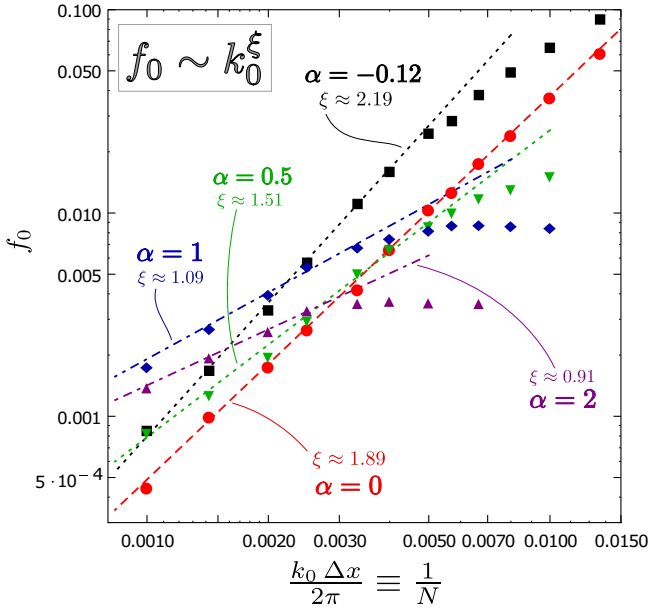

Fig. 12. (Log-log scale) The lowest frequency f_0 dependence on the lowest wave number k_0 in the dynamics of the surface roughness $w(t)$ for several parameter α values. Symbols: calculated values. Lines: power-law fits (with exponent ξ) of the results for small k_0.

in Figure 12 imply that at smaller scales – say, $n_0 < 200$ ($k_0 \Delta x/2\pi > 0.005$ in Fig. 12) – the rate is monotonically decreasing with α. On the other hand, for larger scales, this does not hold any more. For example, for $\alpha = 0$, 0.5, 1 the relation of between f_0 and α reverses (becomes monotonically increasing) already at $n_0 > 300$. For large enough scales, f_0 should become monotonically increasing with α for all values, at least in $-0.12 \leq \alpha \leq 2$, if the power-law trends $f_0(k_0) \propto k_0^{\xi}$ shown as straight lines in Figure 12 continue for even larger systems, $N > 1000$.

5.2 Fits by two generalized Lorentzians

The fits of the PSDs $W(f)$ by a generalized Lorentzian plus a constant (24) seem to be suitable for most cases investigated for $-0.12 \leq \alpha \leq 5$ with system sizes $100 \leq N \leq 1000$. However, for $\alpha = 0.5$ and $\alpha = 1$, and system sizes $N \geq 700$, some larger deviations from the fits can be observed. For example, Figure 13 displays the apparent occurrence of a second hump in the PSD for $\alpha = 1$ at $N = 1000$ which renders the fit (24) less suitable, although at smaller N it works very well (dotted lines in Figure 13). In these cases, however, the sum of two generalized Lorentzians and a constant with the same exponent β,

$$W_{\text{fit}}(f) = \frac{A_1}{(f_{01}^2 + f^2)^{\beta/2}} + \frac{A_2}{(f_{02}^2 + f^2)^{\beta/2}} + B\,, \qquad (26)$$

fits the PSD almost perfectly (orange long-dashed line in Fig. 13 and red dashed line in Fig. 14).

As can be seen in Figure 14, the characteristic frequencies f_{01} and f_{02} of the two-generalized-Lorentzian fit (26)

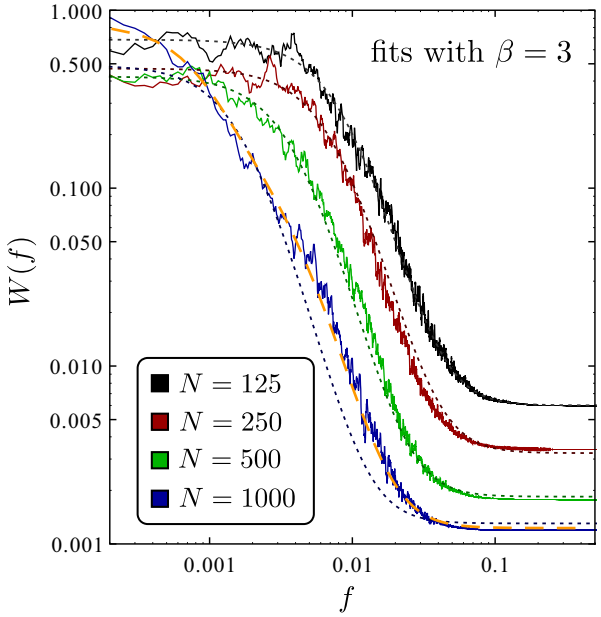

Fig. 13. The PSDs $W(f)$ of $w(t)$ from $t \in [2 \times 10^4, 10^5)$ for $\alpha = 1$ and different system sizes. Solid lines: the calculated PSDs. Dotted lines: single-generalized-Lorentzian (24) fits with exponent $\beta = 3$. Long-dashed orange line: fit of the PSD at $N = 1000$ by two generalized Lorentzians (26) with the same exponent $\beta = 3$.

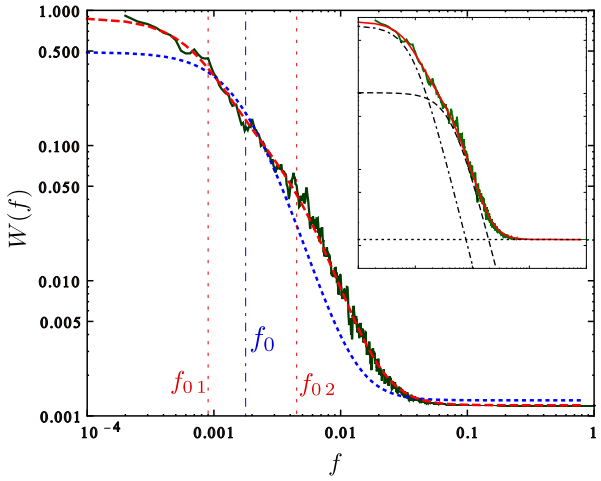

Fig. 14. (Log-log scale) The PSD of the surface roughness $w(t)$ for $\alpha = 1$ and $N = 1000$ (solid dark green line) with fits by a single generalized Lorentzian (24) (dotted blue line) and by a two-generalized-Lorentzian fit (26) (dashed red line), cf. Figure 13. The vertical straight lines indicate the characteristic frequencies f_0, f_{01} and f_{02} of the fits. The inset shows the fit (26) decomposed into two Lorentzians and a constant.

have the frequency f_0 of the original single-generalized-Lorentzian fit (24) between them, i.e., $f_{01} < f_0 < f_{02}$. Moreover, the frequency f_0 seems to follow the power-law trend (blue diamonds and dash-dotted line in Fig. 12), even if the fit is not that good as for smaller N values.

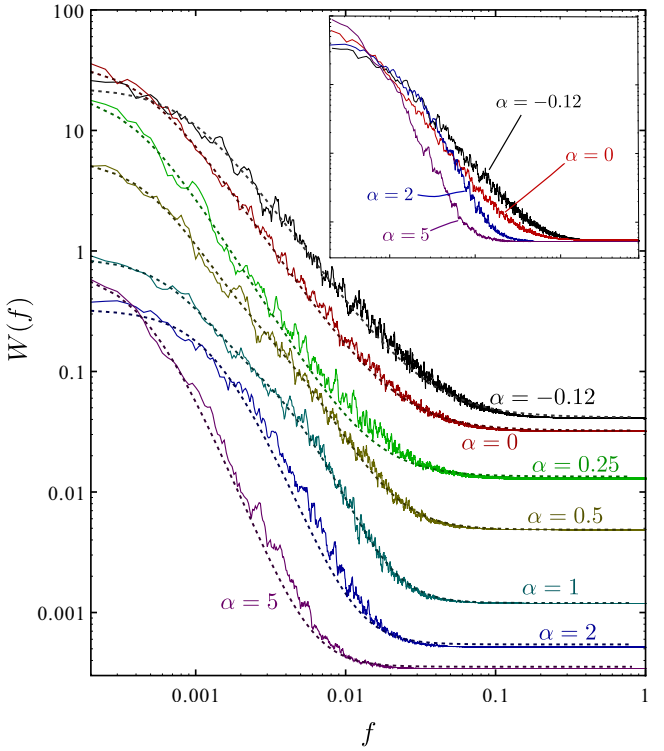

Fig. 15. Power-spectral densities (solid lines) of the surface roughness $w(t)$ for a system size $N = 1000$ and different values of α with their fits (dotted lines): a two-generalized-Lorentzian fit (26) for $\alpha = 0.5$ and $\alpha = 1$, and a single generalized Lorentzian fit (24) for all other values. The inset shows some of the same PSDs normalized.

Figure 15 displays the PSDs with their fits (24) and (26) for the whole parameter α range investigated at system size $N = 1000$.

6 Summary and outlook

The results presented in this paper give some new insights into the complex spatio-temporal behaviour of surfaces produced by the two-dimensional generalized Kuramoto-Sivashinsky equation (1) and might be interesting to a broader circle of researchers working in the field of continuum systems with complex nonlinear dynamics.

The scaling properties (13) of the saturated surface roughness indicate that additional large scale height variations of scale free character appear when the system size N is increased. The dynamics of these slow height variations can be investigated by analysing the time series of the fluctuating surface roughness $w(t)$ where the occurrence of slow modes with increasing system size can also be observed (see Figs. 6 and 7). This analysis shows that the resulting power-spectral densities (PSDs) can be expressed as the sum of a generalized Lorentzian and a constant, (24), or, in some cases, as two generalized Lorentzians (26), as shown in Figures 9, 13 and 15.

The characteristic frequency f_0 obtained as a fit parameter corresponds to the smallest rate (largest time

scale) that plays a role in the surface evolution. It can be attributed to the spatial mode of lowest wave number k_0 (which is inversely proportional to the system size) that can appear in the system. The dependence of this characteristic frequency on the system size gives the "dispersion relation" $f_0(k_0)$ that connects spatial and temporal scales of surface dynamics. These relations have the power-law $f_0 \sim k_0^{\xi}$ character (see Fig. 12) for large systems (small k_0), suggesting that the underlying temporal behaviour is scale free. The exponent ξ is found to decrease with increasing value of parameter α. These results indicate that the dependence of the characteristic time scale of the dynamics on the parameter α changes with the spatial scale: on smaller spatial scales the characteristic time decreases very strongly with increasing α, whereas on large enough spatial scales the evolution is slower for smaller α.

It is hard to make rigorous conclusions regarding the connection between the exponent ξ and the dynamical exponent z found in scaling relations for interfaces (see, e.g. [35,47,55]). However, it is interesting to note that the value $\xi \approx 1.89$ obtained for the KS equation lies between the dynamical exponent values $z = 1.41$ of the KPZ equation and $z = 2$ for Edwards-Wilkinson equation for two dimensions (see [47]).

The findings presented in this paper also raise some interesting questions for further research. For example, it is apparent from Figure 11 and from the values of the PSD exponent β that the character of surface roughness dynamics depends quite strongly on parameter α. The question arises how temporal properties on various scales change with α and what are the statistical properties of the apparent bursts observed for larger values of α.

The Lorentzian shape, $W(f) \sim (f_0^2+f^2)^{-1}$, of the PSD and relation $f_0 \sim k_0^{\xi}$ with $\xi \approx 2$ for $\alpha \approx 0$ also suggests a possible analogy between the large-scale fluctuations of surface roughness and a diffusive process with the probability density Fourier transformed in space and time [56],

$$\hat{P}(k_0, f) \propto \frac{k_0^2}{(k_0^2 D)^2 + f^2},$$

where D is the diffusion constant independent of the system size. This correspondence becomes apparent when $f_0 = Dk_0^2$ is substituted in (21). Thus, perhaps the slow kinetics of the surface roughness might even be reproduced by a random walk of a particle in some external potential which is implied by the fact that the process $w(t)$ is bounded and, consequently, k_0 does not go to zero for systems of finite size. For larger α values where the corresponding PSD exponent $\beta \approx 3$ and $\xi < 2$ this process would then correspond to anomalous diffusion. Moreover, the fact that, for some parameter values, one more generalized Lorentzian has to be added to the in order to fit the calculated PSD for large systems (see Figs. 13 and 14) suggests the emergence of one more time scale, or perhaps, the whole interval of time scales.

These changes in dynamics due to the increase of α can perhaps be attributed to the fact that equation (1) with larger α produces coarser and slower-evolving small-scale patterns (cells or bumps) whose corresponding dynamic time scales begin to significantly overlap with the time scales of the slow height variations. Any conclusive answers about both, the exact character and the occurrence mechanism, of these effects require more analytical work and data obtained from simulations on even larger systems.

In future work, we plan to investigate the transition between the stationary long-time dynamics for small values of parameter α and non-stationary coarsening regime in the large α limit. Another interesting research direction concerns the distributions of surface height, global and local roughness [57–60] and how they change with α and scale with the system size. It would also be useful to know how all of these properties are influenced by noise.

Author contribution statement

V.J. has formulated the initial problem, has carried out the computations, and has written the initial draft of the paper. J.A. has supervised and managed the work. All three authors have equally contributed to the discussion of the results, and the writing of the final version of the manuscript.

References

1. E.C. Harris, *Principles of archaeological stratigraphy* (Elsevier, 2014)
2. G.S. May, S.M. Sze, *Fundamentals of semiconductor fabrication* (John Wiley & Sons, New York, 2004)
3. S. Bae, H. Kim, Y. Lee, X. Xu, J.S. Park, Y. Zheng, J. Balakrishnan, T. Lei, H.R. Kim, Y.I. Song et al., Nat. Nanotechnol. **5**, 574 (2010)
4. M.C. Cross, P.C. Hohenberg, Rev. Mod. Phys. **65**, 851 (1993)
5. M. Castro, R. Cuerno, M. Nicoli, L. Vzquez, J.G. Buijnsters, New J. Phys. **14**, 103039 (2012)
6. M. Hairer, Ann. Math. **178**, 559 (2013)
7. V. Juknevicius, Eur. Phys. J. B **89**, 1 (2016)
8. M. Raible, S. Mayr, S. Linz, M. Moske, K. Samwer et al., Europhys. Lett. **50**, 61 (2000)
9. M. Raible, S.J. Linz, P. Hänggi, Phys. Rev. E **64**, 031506 (2001)
10. M. Raible, S.J. Linz, P. Hänggi, Eur. Phys. J. B: Condens. Matter Complex Syst. **27**, 435 (2002)
11. R. Cuerno, A.L. Barabási, Phys. Rev. Lett. **74**, 4746 (1995)
12. T. Kim, C.M. Ghim, H. Kim, D. Kim, D. Noh, N. Kim, J. Chung, J. Yang, Y. Chang, T. Noh et al., Phys. Rev. Lett. **92**, 246104 (2004)
13. M. Castro, R. Cuerno, L. Vázquez, R. Gago, Phys. Rev. Lett. **94**, 016102 (2005)
14. R. Gago, L. Vázquez, O. Plantevin, T.H. Metzger, J. Muñoz-García, R. Cuerno, M. Castro, Appl. Phys. Lett. **89**, 233101 (2006)

15. R. Cuerno, M. Castro, J. Muñoz-García, R. Gago, L. Vázquez, Nucl. Instrum. Meth. Phys. Res. Sect. B: Beam Interact. Mater. Atoms **269**, 894 (2011)
16. J. Muñoz-García, R. Cuerno, M. Castro, Phys. Rev. E **74**, 050103 (2006)
17. J. Muñoz-García, R. Gago, L. Vázquez, J.A. Sánchez-García, R. Cuerno, Phys. Rev. Lett. **104**, 026101 (2010)
18. G. Sivashinsky, Acta Astronaut. **4**, 1177 (1977)
19. D. Michelson, G. Sivashinsky, Acta Astronaut. **4**, 1207 (1977)
20. G. Sivashinsky, Acta Astronaut. **6**, 569 (1979)
21. Y. Kuramoto, *Chemical oscillations, waves, and turbulence* (Springer-Verlag, 1984)
22. K. Sneppen, J. Krug, M. Jensen, C. Jayaprakash, T. Bohr, Phys. Rev. A **46**, R7351 (1992)
23. C. Jayaprakash, F. Hayot, R. Pandit, Phys. Rev. Lett. **71**, 12 (1993)
24. B.M. Boghosian, C.C. Chow, T. Hwa, Phys. Rev. Lett. **83**, 5262 (1999)
25. M. Paniconi, K. Elder, Phys. Rev. E **56**, 2713 (1997)
26. M. Rost, J. Krug, Phys. Rev. Lett. **75**, 3894 (1995)
27. K.B. Lauritsen, R. Cuerno, H.A. Makse, Phys. Rev. E **54**, 3577 (1996)
28. K. Dreimann, S.J. Linz, Chem. Phys. **375**, 606 (2010)
29. C. Diddens, S.J. Linz, Eur. Phys. J. B **86**, 1 (2013)
30. C. Diddens, S.J. Linz, Eur. Phys. J. B **88**, 1 (2015)
31. V. Yakhot, Phys. Rev. A **24**, 642 (1981)
32. I. Procaccia, M.H. Jensen, V.S. Lvov, K. Sneppen, R. Zeitak, Phys. Rev. A **46**, 3220 (1992)
33. M. Kardar, G. Parisi, Y.C. Zhang, Phys. Rev. Lett. **56**, 889 (1986)
34. M.J. Vold, J. Coll. Sci. **18**, 684 (1963)
35. F. Family, T. Vicsek, J. Phys. A: Math. Gen. **18**, L75 (1985)
36. V. Lvov, I. Procaccia, Phys. Rev. Lett. **72**, 307 (1994)
37. C. Jayaprakash, F. Hayot, R. Pandit, Phys. Rev. Lett. **72**, 308 (1994)
38. M. Nicoli, E. Vivo, R. Cuerno, Phys. Rev. E **82**, 045202 (2010)
39. P. Manneville, H. Chaté, Phys. D: Nonlinear Phenom. **96**, 30 (1996)
40. S.F. Edwards, D. Wilkinson, in *Proceedings of the Royal Society of London A: Mathematical, Physical and Engineering Sciences* (The Royal Society, 1982), Vol. 381, pp. 17–31
41. T. Nattermann, L.H. Tang, Phys. Rev. A **45**, 7156 (1992)
42. M. Raible, S.J. Linz, P. Haenggi, Acta Phys. Pol. B **33**, 1049 (2002)
43. M. Raible, S.J. Linz, P. Hänggi, Phys. Rev. E **62**, 1691 (2000)
44. J. Muñoz-García, R. Cuerno, M. Castro, J. Phys.: Condens. Matter **21**, 224020 (2009)
45. M. Castro, R. Cuerno, Phys. Rev. Lett. **94**, 139601 (2005)
46. W.M. Tong, R.S. Williams, Annu. Rev. Phys. Chem. **45**, 401 (1994)
47. A.L. Barabási, H.E. Stanley, *Fractal concepts in surface growth* (Cambridge University Press, 1995)
48. O. Bikondoa, D. Carbone, V. Chamard, T.H. Metzger, J. Phys.: Condens. Matter **24**, 445006 (2012)
49. G. Palasantzas, Phys. Rev. B **48**, 14472 (1993)
50. J.P. Eckmann, S.O. Kamphorst, D. Ruelle, Europhys. Lett. **4**, 973 (1987)
51. J. Gao, H. Cai, Phys. Lett. A **270**, 75 (2000)
52. N. Marwan, M.C. Romano, M. Thiel, J. Kurths, Phys. Rep. **438**, 237 (2007)
53. H. Kantz, T. Schreiber, *Nonlinear time series analysis* (Cambridge University Press, 2004), Vol. 7
54. A.M. Yaglom, *An introduction to the theory of stationary random functions* (Courier Corporation, 2004)
55. K.B. Lauritsen, H.C. Fogedby, J. Stat. Phys. **72**, 189 (1993)
56. N.G. Van Kampen, *Stochastic processes in physics and chemistry* (Elsevier, 1992), Vol. 1
57. G. Foltin, K. Oerding, Z. Rácz, R.L. Workman, R.K.P. Zia, Phys. Rev. E **50**, R639 (1994)
58. Z. Rácz, M. Plischke, Phys. Rev. E **50**, 3530 (1994)
59. T. Antal, M. Droz, G. Györgyi, Z. Rácz, Phys. Rev. E **65**, 046140 (2002)
60. F.A. Reis, J. Stat. Mech.: Theory Exp. **2015**, P11020 (2015)